Coherence solution for bidirectional reflectance distributions of surfaces with wavelength-scale statistics

Brian G. Hoover

Advanced Optical Technologies, Albuquerque, New Mexico 87198-8383

Victor L. Gamiz

U.S. Air Force Research Laboratory, Directed Energy Directorate, Kirtland Air Force Base, New Mexico 87117–5776

Received April 20, 2005; revised July 18, 2005; accepted August 8, 2005

The scalar bidirectional reflectance distribution function (BRDF) due to a perfectly conducting surface with roughness and autocorrelation width comparable with the illumination wavelength is derived from coherence theory on the assumption of a random reflective phase screen and an expansion valid for large effective roughness. A general quadratic expansion of the two-dimensional isotropic surface autocorrelation function near the origin yields representative Cauchy and Gaussian BRDF solutions and an intermediate general solution as the sum of an incoherent component and a nonspecular coherent component proportional to an integral of the plasma dispersion function in the complex plane. Plots illustrate agreement of the derived general solution with original bistatic BRDF data due to a machined aluminum surface, and comparisons are drawn with previously published data in the examination of variations with incident angle, roughness, illumination wavelength, and autocorrelation coefficients in the bistatic and monostatic geometries. The general quadratic autocorrelation expansion provides a BRDF solution that smoothly interpolates between the well-known results of the linear and parabolic approximations.

OCIS codes: 030.5770, 290.5880.

1. INTRODUCTION

The bidirectional reflectance distribution function (BRDF) describes one of the most basic optical phenomena: the average angular distribution of intensity reflected by a macroscopically planar, generally random medium or surface illuminated by a plane wave incident from a specified direction. Under coherent laser illumination, provided that the illuminated area is much larger than the scale of spatial inhomogeneities of the medium or surface, the BRDF represents the radiant or angular intensity envelope under which the speckle pattern occurs. The BRDF is of fundamental importance in diverse applications including data simulation and analysis in both laser radar[1–3] and passive photometry[4–6] of solid targets, laser industrial process control,[7] high-energy laser (HEL) control,[8] stray-light analysis,[9] illumination design,[10] and computer vision,[11,12] animation,[13] and virtual reality.[14–17]

Theoretical models describe the dependence of the BRDF on the physical properties of the reflector, which for surfaces may include the surface height distribution, height autocorrelation, slope distribution, and optical constants. Models are typically valid over limited parameter domains, with the most common delimiting surface parameter being the effective roughness

$$\sigma \equiv \sigma_h/\lambda, \tag{1}$$

where σ_h is the standard deviation of the surface height distribution and λ is the illumination wavelength.[18,19] Rigorous numerical models have been developed within limited domains of the surface autocorrelation length a, for instance in the limit $2\pi a/\lambda \to \infty$.[20] Several recent reviews survey surface BRDF models within their respective ranges of validity.[21,22] The most widely used models, which are all approximate analytical as opposed to numerical models, are summarized below in order to provide background for the developments of this paper.

Several surface BRDF models are well established in the roughness domain $\sigma \ll 1$, which encompasses very smooth, mirrorlike surfaces. The most widely used is the Rayleigh–Rice model, which gives the BRDF as proportional to the power spectral density of the random process that describes the surface heights.[23–25] Other prominent models in the small-roughness domain are based on perturbation theory[25] and on the Ewald–Oseen extinction theorem,[25,26] the latter of which is also applicable in numerical studies of rougher surfaces.[27]

Several analytical BRDF models have been developed in the large-roughness domain $\sigma \gtrsim 1$, although none has enjoyed very wide application, presumably due to a combination of limited accuracy and difficulty of implementation. Beckmann provided the seminal BRDF model in the large-roughness domain by averaging the Kirchhoff diffraction integral of a generalized surface over the statistical ensemble of surface realizations.[28] The Beckmann model, which is also referred to as the Kirchhoff or physical-optics model, specifies the surface field by using the tangent-plane approximation, which assumes that each point on the surface has a unique normal relative to

which a tangent plane can be assigned, and is therefore generally applicable only to surface features with radii of curvature sufficiently larger than the illumination wavelength. In particular, surface profiles with discontinuous derivatives are formally inadmissible under the tangent-plane approximation, although pyramidal features with facet dimensions $\sim 10\lambda$ have been accurately described by the Beckmann model.[29] Extensions of the Beckmann model in the field of computer-graphic design have contributed treatments of polarization and shadowing effects.[30] The Stratton–Chu–Silver integral[31] was applied to optical scattering by Leader,[32,33] with the surface fields also determined under the tangent-plane approximation. These models, as well as that developed in this paper, are valid for large effective roughness $\sigma \gtrsim 1$ in the absence of multiple scattering. For a specified σ_h the restriction on multiple scattering implies a proportional lower bound on the autocorrelation length a.

Despite the development of diffractive BRDF models at various levels of rigor, many applications still rely on scattering models based on geometrical optics. The stationary-phase solution of the physical-optics integral leads to specular-point or microfacet BRDF models,[34–37] which also rely on the tangent-plane approximation but neglect diffraction, which, while affording simplicity of application, also limits validity and flexibility. Microfacet models cannot, for instance, consistently account for BRDF variations with roughness or wavelength, nor other diffractive effects.

In this paper a scalar diffractive BRDF model valid for surfaces with large effective roughness $\sigma \gtrsim 1$ is developed from optical coherence theory and a reflective phase-screen model. Departure from the tangent-plane approximation, enabled in this case by the phase-screen approximation, allows consideration of general surfaces with large and/or discontinuous slopes. The tangent-plane approximation is shown to be actually incompatible with the coherence approach to the scattering problem (see Subsection 2.A). Surfaces with large slopes and large effective roughness fall outside of the ranges of applicability of the most popular approximate analytical models as mentioned above.[22,38] The basis of the current model in coherence theory provides a BRDF solution consistent and interpretable within a classical framework, one result of which is the clarification of the coherence properties of scattered fields (see Subsection 2.B). A second benefit of the coherence approach is compatibility with a variety of results from coherence theory potentially relevant to scattering analysis, for instance with recent developments in electromagnetic coherence theory.[39–41]

A general quadratic expansion of the surface autocorrelation function near the origin is used to derive an integral solution for the general BRDF due to a perfectly conducting surface with arbitrary two-dimensional isotropic roughness $\sigma \gtrsim 1$. The general solution consists of an incoherent component that varies with the scattered elevation angle as $\cos \theta_s$, irrespective of the incident angle, plus a nonspecular coherent component proportional to the azimuthal integral of the Faddeeva or plasma dispersion function over the surface. The plasma dispersion function is related to the complex error function and the Voight profile and arises in many areas of mathematical physics.[42–44] When evaluated with representative autocorrelation types, the general solution yields the Cauchy and Gaussian BRDFs, which are forms commonly employed in empirical fitting routines.[45] The general solution is seen to smoothly interpolate between these well-known forms. The large majority of BRDF models that rely on expansion of the surface autocorrelation function use the parabolic approximation, which forces a Gaussian BRDF solution. While several models have been based on the linear approximation,[46,47] this paper is apparently the first to derive the BRDF on the assumption of an autocorrelation arbitrary to second order. Inclusion of the gradient in the autocorrelation expansion generally improves agreement with data due to surfaces with large slopes, including planetary surfaces[48–50] and machined surfaces (see Subsection 3.A). It is argued in Subsections 2.B and 3.A that the general solution overcomes long-standing objections to the well-known BRDF forms provoked by energy conservation and the linear autocorrelation approximation.[25,51,52]

For practical reasons only surfaces in the so-called resonant domain $a \sim \lambda$ are examined in detail. Due to the restriction on multiple scattering, the surface roughness is therefore likewise limited as $\sigma \sim 1$. The surface statistics are on the scale of the wavelength. The integral for the general BRDF solution is evaluated and plotted by using Mathematica 5. Plots illustrate the agreement of the general solution with original bistatic specular-plane BRDF data due to a machined aluminum surface, and its variation with incident angle, surface roughness, illumination wavelength, and autocorrelation coefficients in the bistatic and monostatic geometries. Out-of-plane scattering is illustrated in full-hemisphere plots for several surfaces. The plots are, where possible, compared qualitatively with previously published data due to surfaces with similar statistics.

2. DERIVATION

In this section the general scalar surface BRDF solution is derived in the limit $\sigma \gtrsim 1$. The requisite theoretical background is summarized, including Goodman's derivation of the coherence function on a random reflective phase screen.[53] A general quadratic series expansion of the surface autocorrelation appropriate for $\sigma \gtrsim 1$ is applied, and the BRDF integral is specified for anisotropic roughness. Under the assumption of isotropic roughness, with two representative autocorrelation types, this integral is shown to produce BRDF forms commonly observed in measurements. The general BRDF integral for the isotropically rough surface is cast as an integral of the Faddeeva or plasma dispersion function, several plots of which are given as encountered in scattering calculations.

The units of the BRDF are sr^{-1}. The BRDF is related to the ensemble-average radiant intensity distribution by

$$\mathrm{BRDF}(\mathbf{k}_s, \mathbf{k}_i) = \langle I(\mathbf{k}_s, \mathbf{k}_i) \rangle / P_i \cos \theta_s, \tag{2}$$

where $\mathbf{k}_{s,i}$ is the reflected/scattered or incident wave vector, respectively, P_i is the uniform incident power, and θ_s is the elevation of the scattered wave vector measured from the average surface normal. The units of $\langle I(\mathbf{k}_s, \mathbf{k}_i) \rangle$ are W/sr.[54] Equation (2) specifies the BRDF as an average

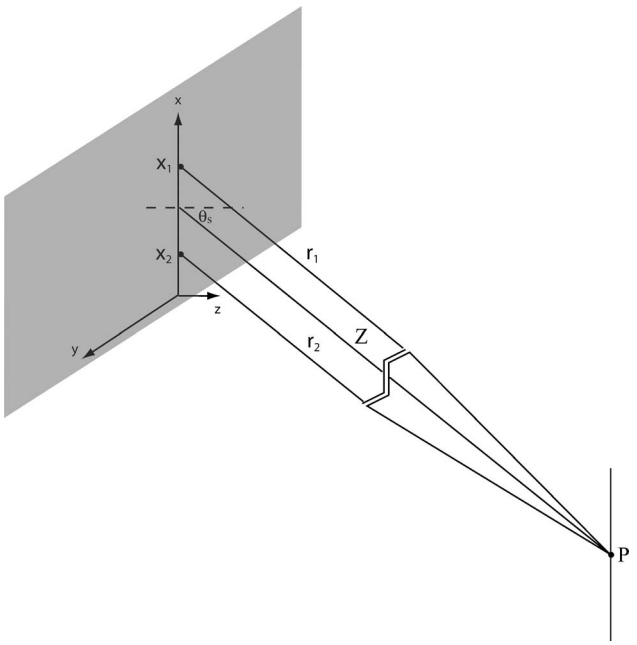

Fig. 1. Geometry and notation relevant to derivation of the BRDF at point P from the coherence between the surface points $\mathbf{x}_1$ and $\mathbf{x}_2$. $\Delta\mathbf{x}=\mathbf{x}_1-\mathbf{x}_2$.

over an ensemble of independent, identically distributed (IID) rough surfaces, which is typically realized in practice under the ergodic criterion as an average over a measurement parameter such as in-plane surface displacement or rotation. In this paper the average radiant intensity is referred to simply as the BRDF, although the conversion of Eq. (2) must be applied to the results to recover the conventional radiometric quantity. Plotted results are given as radiant intensity with specified normalizations.

A. Coherence-Theory Background

The application of coherence theory to the description of radiometric properties of certain types of primary radiation sources has been well described.[55–57] In the treatment of qualified illuminated surfaces as secondary sources, statistical moments of scattered fields over ensembles of surfaces are applied as coherence functions for general analyses.[58] The present derivation utilizes the second moment of the field scattered by a random, perfectly conducting phase screen with a Gaussian distribution of surface heights.[53] This approach has been applied recently to the derivations of BRDF solutions for several surface types.[59,60]

The surface illumination is idealized as a quasi-monochromatic plane wave, which allows application of the generalized Van Cittert–Zernike (VCZ) theorem to the mutual intensity (coherence) function on the surface. The generalized VCZ theorem relates the BRDF to the mutual intensity through a Fourier transform, provided that the surface field is quasi-homogeneous.[55,56,61] The quasi-homogeneous assumption is satisfied when the spatial scale of amplitude variations is much larger than the spatial scale of coherence variations of the field, as will occur on a surface with large effective roughness $\sigma\gtrsim 1$ when the size of the illuminated area is much larger than the scale of spatial inhomogeneities. As demonstrated in Appendix A, the average scattered radiant intensity as a function of wave vector is then given by the generalized VCZ theorem as

$$\langle I(\bar{\mathbf{k}}_s)\rangle = \frac{\mathcal{A}\bar{M}_r \cos^2\theta_s}{\bar{\lambda}^2}\int\int \gamma(\Delta\mathbf{x})\exp(-j\bar{\mathbf{k}}_s\cdot\Delta\mathbf{x})\mathrm{d}\Delta\mathbf{x}, \tag{3}$$

where $\bar{\mathbf{k}}_s$ is the wave vector associated with scattered quasi-monochromatic light of center wavelength $\bar{\lambda}$, $\mathcal{A}$ is the illuminated area, $\bar{M}_r$ is the average reflected emittance (also known as exitance) over the surface, and $\gamma(\Delta\mathbf{x})$ is the normalized mutual intensity on the surface as a function of directed spatial separation.[62] Dependence of $\bar{M}_r$ and $\gamma(\Delta\mathbf{x})$ on the incident wave vector is implicit in Eq. (3). For application of Eq. (3) the average surface is taken to be coincident with the xy plane, and the scattered wave vector is restricted to the xz plane. Equation (3) provides the BRDF over the entire reflected hemisphere by rotation of the surface and the vector argument $\Delta\mathbf{x}=\hat{\mathbf{x}}\Delta x+\hat{\mathbf{y}}\Delta y$ of the mutual intensity function about the z axis. The geometry of Eq. (3) is illustrated in Fig. 1.

The derivation places several restrictions on the surface in addition to $\sigma\gtrsim 1$, primarily that neither shadowing nor multiple scattering can occur. Following Goodman,[53] the field at the surface is expressed as a function of the surface height $h(\mathbf{x})$ as

$$u(\mathbf{x}) = a(\mathbf{x})\exp(j\bar{\mathbf{k}}_i\cdot\mathbf{x})\exp\left[\frac{2\pi j}{\bar{\lambda}}(1+\cos\theta_i)h(\mathbf{x})\right]$$
$$= a(\mathbf{x})\exp(j\bar{\mathbf{k}}_i\cdot\mathbf{x})\exp[j\alpha(\mathbf{x})], \tag{4}$$

where $a(\mathbf{x})$ is the scattered amplitude and $\bar{\mathbf{k}}_i$ is the center wave vector incident at the elevation angle θ_i relative to the average surface normal. Figure 2 illustrates the geometry of Eq. (4).

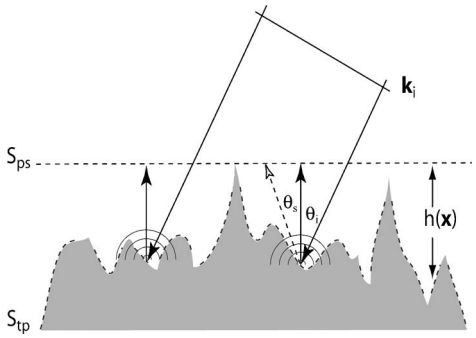

Fig. 2. Illustration of the phase-screen approximation of the scattered field on the rough surface. The field is specified on the virtual surface S_{ps} just above the actual surface, in contrast with the tangent-plane approximation in which the field is specified on the surface facets S_{tp}, where the radius of curvature is sufficiently larger than the wavelength. The phase difference due to a lateral separation of surface points is $\mathbf{k}_i\cdot\mathbf{x}$, while the phase difference due to the surface height $h(\mathbf{x})$ is $kh(\mathbf{x})(1+\cos\theta_i)$. The angle θ_s is not relevant in the phase-screen approximation as it is in the tangent-plane approximation.

As shown in Fig. 2, the surface on which the scattered field is specified under the phase-screen approximation (S_{ps}) differs from that under the tangent-plane approximation (S_{tp}). Both approximations are based on application of the Helmholtz integral[28] but differ in the boundary surface on which the field is specified. Under the tangent-plane approximation the term $1+\cos\theta_i$ in Eq. (4) is replaced by $\cos\theta_s+\cos\theta_i$, a distinction that affects not only the model solution but also the fundamental interpretation of the scattering process. Since it depends on both surface position $\mathbf{x}$ and scattering direction θ_s, the second moment of the field under the tangent-plane approximation is a *radiance* function and therefore inadmissible as a coherence function in Eq. (3).[57] The implications of this fundamental incompatibility should be fully appreciated through further investigations.

From Eq. (4) the phase variance and phase autocorrelation of the scattered field are

$$\sigma_\alpha^2 = [2\pi\sigma(1+\cos\theta_i)]^2, \tag{5}$$

$$R_\alpha(\Delta\mathbf{x}) = \left[\frac{2\pi}{\bar{\lambda}}(1+\cos\theta_i)\right]^2 R_h(\Delta\mathbf{x}), \tag{6}$$

respectively, where $R_h(\Delta\mathbf{x})$ is the autocorrelation of the two-dimensional random process that describes the surface heights. In Eq. (4) the amplitude $a(\mathbf{x})$ and the phase $\alpha(\mathbf{x})$ are assumed to be uncorrelated, allowing the normalized mutual intensity to be expressed as

$$\gamma(\Delta\mathbf{x}) \equiv \frac{\langle u(\mathbf{x})u^*(\mathbf{x}-\Delta\mathbf{x})\rangle}{\sqrt{\langle u^2(\mathbf{x})\rangle\langle u^2(\mathbf{x}-\Delta\mathbf{x})\rangle}} = \frac{\exp(j\bar{\mathbf{k}}_i\cdot\Delta\mathbf{x})}{\langle a^2(\mathbf{x})\rangle}\langle a(\mathbf{x})a(\mathbf{x}-\Delta\mathbf{x})\rangle\langle\exp\{j[\alpha(\mathbf{x})-\alpha(\mathbf{x}-\Delta\mathbf{x})]\}\rangle, \tag{7}$$

where the quasi-homogeneous assumption allows simplification of the denominator. Under the conventional phase-screen approximation the scattered amplitude $a(\mathbf{x})$ varies with $\mathbf{x}$ much more slowly than does the phase $\alpha(\mathbf{x})$, in which case the normalized mutual intensity on the rough surface becomes

$$\gamma(\Delta\mathbf{x}) = \exp(j\bar{\mathbf{k}}_i\cdot\Delta\mathbf{x})\langle\exp\{j[\alpha(\mathbf{x})-\alpha(\mathbf{x}-\Delta\mathbf{x})]\}\rangle. \tag{8}$$

Because the conventional phase-screen approximation assumes that every point on the surface responds identically to the incident field, it should be more accurate in specifying an electromagnetic scattered field component perpendicular to the incident plane (s polarization) than a component parallel to the incident plane (p polarization). This is an important consideration in comparison of the results of the scalar model with data.

The ensemble average in Eq. (8) can be evaluated by using the second-order characteristic function with a Gaussian distribution of surface heights to yield

$$\gamma(\Delta\mathbf{x}) = \exp(j\bar{\mathbf{k}}_i\cdot\Delta\mathbf{x})\exp\{-\sigma_\alpha^2[1-\rho_h(\Delta\mathbf{x})]\}, \tag{9}$$

where $\rho_h(\Delta\mathbf{x}) \equiv R_h(\Delta\mathbf{x})/\sigma_h^2$ is the normalized surface autocorrelation function.[53] Substitution of this result into the VCZ theorem of Eq. (3) provides the BRDF as

$$\langle I(\bar{\mathbf{k}}_s,\bar{\mathbf{k}}_i)\rangle = \frac{\mathcal{A}\bar{M}_r\cos^2\theta_s}{\bar{\lambda}^2}\int\int \exp\{-\sigma_\alpha^2[1-\rho_h(\Delta\mathbf{x})]\} \times\exp[j(\bar{\mathbf{k}}_i-\bar{\mathbf{k}}_s)\cdot\Delta\mathbf{x}]\mathrm{d}\Delta\mathbf{x}. \tag{10}$$

With $\Delta\bar{\mathbf{k}}\equiv\bar{\mathbf{k}}_i-\bar{\mathbf{k}}_s$, $\Delta\bar{\mathbf{k}}\cdot\Delta\mathbf{x}$ represents the scattered wavevector distance from the direction of specular reflection. In circular polar coordinates the BRDF expression becomes

$$\langle I(\bar{\mathbf{k}}_s,\bar{\mathbf{k}}_i)\rangle = \frac{\mathcal{A}\bar{M}_r\cos^2\theta_s}{\bar{\lambda}^2}\int_0^\infty\int_0^{2\pi} \times\exp\{-\sigma_\alpha^2[1-\rho_h(\Delta\mathbf{x})]\} \times\exp[j(\Delta\bar{\mathbf{k}}\cdot\Delta\mathbf{x})]r\mathrm{d}\varphi\mathrm{d}r, \tag{11}$$

with the integration understood to cover the plane of coordinate *differences* on the surface. In the coordinate system (r,φ) we have

$$\Delta\bar{\mathbf{k}}\cdot\Delta\mathbf{x} = -\bar{k}r(A\cos\varphi + B\sin\varphi), \tag{12}$$

with $A\equiv\sin\theta_s\cos\phi_s+\sin\theta_i\cos\phi_i$ and $B\equiv\sin\theta_i\sin\phi_i$, the subscripts i and s referring to the incident and scattered wave vectors. The azimuth angle $\phi_{i(s)}$ of the incident (scattered) plane wave should be distinguished from the surface azimuth φ. The ranges of θ and ϕ_i are $[0,\pi/2]$ and $(-\pi,\pi]$, respectively, and $\phi_s=0$ or π, with $\bar{\mathbf{k}}_s$ confined to the xz plane. These are standard notations in the description of BRDF instrumentation.[63]

B. Large-Roughness Approximation

Series expansion of the surface autocorrelation $\rho_h(\Delta\mathbf{x})$ in the limit of large effective roughness $\sigma\gtrsim 1$ allows the integral of Eq. (11) to be developed for an arbitrary autocorrelation and evaluated for a general isotropic autocorrelation. With reference to Eq. (9), since for large σ_α^2 the mutual intensity falls off rapidly as $\rho_h(\Delta\mathbf{x})$ decreases from $\rho_h(0)=1$, an approximation valid for large effective roughness is provided by expansion of $\rho_h(\Delta\mathbf{x})$ for small arguments. The dependence of the mutual intensity on $\rho_h(\Delta\mathbf{x})$ is, however, generally not entirely evident in an expansion centered on the origin $\Delta\mathbf{x}=0$, since by definition $\rho_h(\Delta\mathbf{x})$ is an even function with $\rho_h(0)=1$, which for a general surface implies that the gradient $\nabla\rho_h$ vanishes in a point singularity at the origin. Due largely to this singularity, the autocorrelation expansion has been controversial among scattering theorists,[64] which may explain why the general quadratic expansion has apparently not appeared earlier. Our position that the singularity can be ignored is based less on mathematical than on physical intuition. To avoid the singularity, we expand the autocorrelation about the vector $\varepsilon\Delta\mathbf{x}$ in the limit $\varepsilon\to 0$.

1. Anisotropic Roughness

The normalized surface autocorrelation is expanded in two dimensions as[65]

$$\rho_h(\Delta\mathbf{x}) \cong 1 + \lim_{\varepsilon\to 0}\Big[\ \Delta\mathbf{x}\cdot\nabla\rho_h]_{\varepsilon\Delta\mathbf{x}} + \tfrac{1}{2}\ (\Delta\mathbf{x}\cdot\nabla)(\Delta\mathbf{x}\cdot\nabla\rho_h)]_{\varepsilon\Delta\mathbf{x}}\Big]. \tag{13}$$

Application of the gradient operator in circular polar coordinates and adoption of the shorthand notation $\partial_s\rho_h \equiv \lim_{\varepsilon\to 0}(\ \partial\rho_h/\partial s]_{\varepsilon\Delta\mathbf{x}})$, where $s=r$ or φ, leads to

$$\rho_h(\Delta\mathbf{x}) \cong 1 + r(\partial_r\rho_h) + \frac{\varphi}{r}(\partial_\varphi\rho_h) + \frac{r^2}{2}(\partial_{rr}\rho_h) + \frac{\varphi^2}{2r^2}(\partial_{\varphi\varphi}\rho_h) + \varphi(\partial_{r\varphi}\rho_h). \tag{14}$$

The derivatives $\partial_r\rho_h, \partial_\varphi\rho_h, \ldots$ are functions of the azimuth angle φ in the case of general anisotropic roughness. Substitution from Eq. (12) and relation (14) into Eq. (11) provides an integral expression for the BRDF of a general anisotropically rough surface with $\sigma \gtrsim 1$. Evaluation of this integral is generally difficult due to the mixed terms in relation (14) and the azimuthal dependence of the derivatives, although it might be simplified by approximation of the autocorrelation by planar wedges over azimuthal intervals. The prevalence of anisotropic roughness in processed surfaces should motivate future investigation of the general theory; however, in this paper subsequent attention is limited to isotropic roughness.

2. Isotropic Roughness

A surface with isotropic roughness is described by a surface autocorrelation with azimuthal symmetry, for which all derivatives with respect to φ vanish. In this case substitution from Eq. (12) and relation (14) into Eq. (11) provides the BRDF as

$$\langle I(\bar{\mathbf{k}}_s,\bar{\mathbf{k}}_i)\rangle \cong \frac{\mathcal{A}\bar{M}_r\cos^2\theta_s}{\bar{\lambda}^2}\int_0^\infty\int_0^{2\pi} \times\exp[-j\bar{k}r(A\cos\varphi + B\sin\varphi)]\mathrm{d}\varphi \times\exp\left[\sigma_\alpha^2(\partial_r\rho_h)r + \frac{\sigma_\alpha^2}{2}(\partial_{rr}\rho_h)r^2\right]r\mathrm{d}r, \tag{15}$$

with A and B as defined following Eq. (12). Note that the derivatives $\partial_r\rho_h$ and $\partial_{rr}\rho_h$ are constants on an isotropically rough surface. The integral over azimuth is evaluated by introducing the variables ξ and ψ such that $A=\xi\cos\psi$ and $B=\xi\sin\psi$, which leads to[66]

$$\int_0^{2\pi}\exp[-j\bar{k}\xi r\cos(\varphi-\psi)]\mathrm{d}\varphi = 2\pi J_0(\bar{k}\xi r), \tag{16}$$

where J_0 is the zeroth-order Bessel function and

$$\xi = \sqrt{\sin^2\theta_s + \sin^2\theta_i + 2\sin\theta_i\sin\theta_s\cos\phi_i\cos\phi_s} \tag{17}$$

is the bidirectional independent variable of the BRDF.

Substitution of the result of Eq. (16) into relation (15) leaves the BRDF expression

$$\langle I(\bar{\mathbf{k}}_s,\bar{\mathbf{k}}_i)\rangle \cong \frac{2\pi\mathcal{A}\bar{M}_r\cos^2\theta_s}{\bar{\lambda}^2}\exp(\beta v^2)\int_0^\infty rJ_0(\bar{k}\xi r) \times\exp[-\beta(r+v)^2]\mathrm{d}r \tag{18}$$

after completing the square in the exponent and setting

$$v \equiv \partial_r\rho_h/\partial_{rr}\rho_h, \tag{19}$$

$$\beta \equiv \sigma_\alpha^2|\partial_{rr}\rho_h|/2. \tag{20}$$

The integral in relation (18) is the Fourier–Bessel or zeroth-order Hankel transform of a shifted Gaussian function.[67] The radial derivatives of the isotropically rough surface are hereafter represented in the simplified notation $\rho_1 \equiv \partial_r\rho_h$ and $\rho_2 \equiv \partial_{rr}\rho_h$.

It is instructive to examine the representative forms of the BRDF solution as the derivatives ρ_1 and ρ_2 individually go to 0. With $\rho_1=0$ the solution of relation (18) leads transparently to the Gaussian BRDF[68]

$$\langle I(\bar{\mathbf{k}}_s,\bar{\mathbf{k}}_i)\rangle \cong \frac{\pi\mathcal{A}\bar{M}_r\cos^2\theta_s}{\bar{\lambda}^2\beta}\exp\left[-\frac{(\bar{k}\xi)^2}{4\beta}\right], \tag{21}$$

which is consistent with models that neglect the role of the gradient $\nabla\rho_h$ by assuming a Gaussian surface autocorrelation function. With $\rho_2=0$ the variable v cannot be used. Returning in this case to relation (15) and Eq. (16) yields the Cauchy BRDF[69]

$$\langle I(\bar{\mathbf{k}}_s,\bar{\mathbf{k}}_i)\rangle \cong \frac{2\pi\mathcal{A}\bar{M}_r\cos^2\theta_s}{\bar{\lambda}^2}\frac{\sigma_\alpha^2|\rho_1|}{[\sigma_\alpha^4\rho_1^2 + (\bar{k}\xi)^2]^{3/2}}. \tag{22}$$

The Cauchy BRDF is commonly observed in data due to surfaces with large slopes[48–50] and as a result is commonly employed in empirical fitting routines.[45]

The results of relations (21) and (22) suggest a useful classification, according to the shape of the surface autocorrelation, of isotropically rough surfaces that satisfy the assumptions of the model. Such surfaces with $|\rho_2| > |\rho_1|$ will be referred to as Gaussian-like surfaces, while those with $|\rho_1| > |\rho_2|$ will be referred to as Cauchy-like surfaces, although the actual functional form of the general BRDF solution will generally differ significantly from the representative forms of relations (21) and (22).

General BRDF solution for isotropic roughness in terms of the plasma dispersion function. The integral of relation (18) can be recast as an integral of the Faddeeva or plasma dispersion function over a horizontal contour in the complex plane. The resulting solution suggests a decomposition of the BRDF into coherent and incoherent components as well as a mathematical analogy between wave scattering from rough surfaces and wave propagation in hot, underdense plasmas.[70] The integrals considered are also similar to those encountered in the analysis of generalized Bessel–Gauss beams.[72]

The Fourier–Bessel or zeroth-order Hankel transform of an arbitrary circularly symmetric function $g(r)$ is[67,73]

$$\mathcal{B}\{g(r)\} = \mathcal{G}(R) = \int_0^\infty r J_0(Rr) g(r) \mathrm{d}r. \tag{23}$$

Expressing the Bessel function in its integral form, as in Eq. (16), and changing the order of integrations in relation (18) gives

$$\begin{aligned}\mathcal{B}\{\exp[-\beta(r+v)^2]\} &= \mathcal{G}(R) \\ &= \frac{1}{2\pi}\int_0^{2\pi}\int_0^\infty r \exp(-jRr\cos\varphi) \\ &\quad \times \exp[-\beta(r+v)^2]\mathrm{d}r\mathrm{d}\varphi \\ &= \frac{1}{2\pi}\int_0^{2\pi} \mathcal{G}_1(R\cos\varphi)\mathrm{d}\varphi,\end{aligned} \tag{24}$$

where the subscript 1 denotes the one-dimensional transform and $R=\bar{k}\xi$ from relation (18). With the use of the shorthand notation $X \equiv \bar{k}\xi\cos\varphi$, standard substitution methods with $t=\sqrt{\beta}(r+v+jX/2\beta)$ lead to

$$\mathcal{G}_1(X) = \frac{1}{\beta}\exp(-\beta v^2 - \Gamma^2)\left[\int_{-j\Gamma}^\infty t\exp(-t^2)\mathrm{d}t + \sqrt{\beta} \times \left(v + \frac{jX}{2\beta}\right)\int_{-j\Gamma}^\infty \exp(-t^2)\mathrm{d}t\right], \tag{25}$$

where

$$\Gamma \equiv jv\sqrt{\beta} - \frac{X}{2\sqrt{\beta}}. \tag{26}$$

The contour of integration in Eq. (25) is a line parallel to the real axis in the right half of the complex plane. The first integral in Eq. (25) produces $\frac{1}{2}\exp(\Gamma^2)$, the terms in X of which cancel with the prefactor, while the second integral is the complementary complex error function $\sqrt{\pi}\,\mathrm{erfc}(-j\Gamma)/2$.[42] Slight rearrangement leads to

$$\begin{aligned}\mathcal{G}_1(X) &= \frac{\exp(-\beta v^2)}{2\beta}\left[1 - \sqrt{\pi\beta}\left(v + \frac{jX}{2\beta}\right)\exp(-\Gamma^2)\mathrm{erfc}(-j\Gamma)\right] \\ &= \frac{\exp(-\beta v^2)}{2\beta}\left[1 - \sqrt{\pi\beta}\left(v + \frac{jX}{2\beta}\right)w(\Gamma)\right],\end{aligned} \tag{27}$$

where $w(z)=K(z)+jL(z)$ is the Faddeeva or plasma dispersion function.[42–44,70,71] Inserting the expression for $\mathcal{G}_1$ back into Eq. (24), we express the Fourier–Bessel transform as

$$\begin{aligned}\mathcal{G}(R) &= \frac{\exp(-\beta v^2)}{2\beta}\left[1 - \sqrt{\frac{\beta}{\pi}}\int_0^\pi \left(v + \frac{j\bar{k}\xi\cos\varphi}{2\beta}\right)w(\Gamma)\mathrm{d}\varphi\right] \\ &= \frac{\exp(-\beta v^2)}{2\beta}\left[1 + \frac{\bar{k}\xi}{2\sqrt{\pi\beta}}\int_0^\pi L(\Gamma)(\cos\varphi)\mathrm{d}\varphi\right],\end{aligned} \tag{28}$$

where the final equality follows because $w(\Gamma)$ is analytic and Hermitian along the horizontal contour in the upper half of the complex plane.[44,70]

Inserting Eq. (28) into relation (18) gives the general BRDF solution for the isotropically rough surface as

$$\langle I(\bar{\mathbf{k}}_s, \bar{\mathbf{k}}_i)\rangle \cong \frac{\pi\mathcal{A}\bar{M}_r\cos^2\theta_s}{\bar{\lambda}^2\beta}\left[1 + \frac{\bar{k}\xi}{2\sqrt{\pi\beta}}\int_0^\pi L(\Gamma)(\cos\varphi)\mathrm{d}\varphi\right]. \tag{29}$$

The solution of relation (29) is a sum of incoherent and coherent terms. The incoherent term produces an average radiant intensity proportional to $\cos^2\theta_s$ (*not* $\cos\theta_s$, as for a Lambertian source),[74] which leaves the integral of the plasma dispersion function to represent the BRDF due to coherence on the surface. Calculations of $L(z)$ have been plotted in several references.[44,70] $L(z)$ tends to 0 as the real part of its argument goes to 0 in the upper half of the complex plane [$\mathrm{Im}(z)>0$]. With $\mathrm{Re}\,\Gamma \propto 1/\sigma_h\sqrt{|\rho_2|}$, relation (29) therefore implies that the derived BRDF converges to the incoherent solution $(\pi\mathcal{A}\bar{M}_r\cos^2\theta_s)/\bar{\lambda}^2\beta$ for surfaces with sufficiently narrow autocorrelation or sufficiently large roughness. Referring to Eq. (9), the mutual intensity associated with the incoherent solution is quite narrow as expected. Coherence theory reveals that associated with a general coherence function are both propagating (low-frequency) and nonpropagating or evanescent (high-frequency) components.[74–76] It has been demonstrated that the partition of energy between propagating and evanescent components varies smoothly between the incoherent and coherent limits of a Gaussian coherence function.[75] Since the BRDF solution accounts for the propagating component only, these results from coherence theory imply that the BRDF should not be expected to conserve energy. The factor β in the denominator of relation (29) ensures that the BRDF solution does not conserve energy with variations in roughness or autocorrelation width. Relation (29) specifically predicts that the incoherent BRDF solution vanishes, i.e., that the field scattered from such a surface is purely evanescent, due to the limit $\beta\to\infty$ as $\rho_h(\Delta\mathbf{x})\to\delta(\Delta\mathbf{x})$.[77] To reiterate, contrary to objections in the scattering literature,[51,52] the BRDF does not conserve energy in general, and the energy in the solution derived here varies smoothly with the parameter β.

Computer routines for the numerical calculation of $L(z)$ are readily available,[44,78] although the variable dependences implied by Eq. (26) and relation (29) must be carefully specified. The most suitable routine will depend on the application, in particular on whether the solution of the forward or the inverse scattering problem is required. In the forward problem the BRDF is computed for specified surface parameters, while the inverse problem requires a search algorithm to find surface parameters that provide the best fit to data. A comparison of algorithms available for $L(\Gamma)$ is beyond the scope of this paper—here the built-in complex error function routine in Mathematica 5 (Ref. 78) is utilized for calculation of the plasma dispersion function and the BRDF integral of relation (29). Figures 3 and 4 illustrate results of the Mathematica 5 routine in contour plots of the integrand $\xi L(\Gamma)\times(\cos\varphi)/\sqrt{\beta}$ of the coherent component of the general solution [relation (29)] for two scattering geometries and two sets of surface parameters. In these figures white corresponds to 0, black corresponds to the minimum integrand value, and contours are drawn at consistent inte-

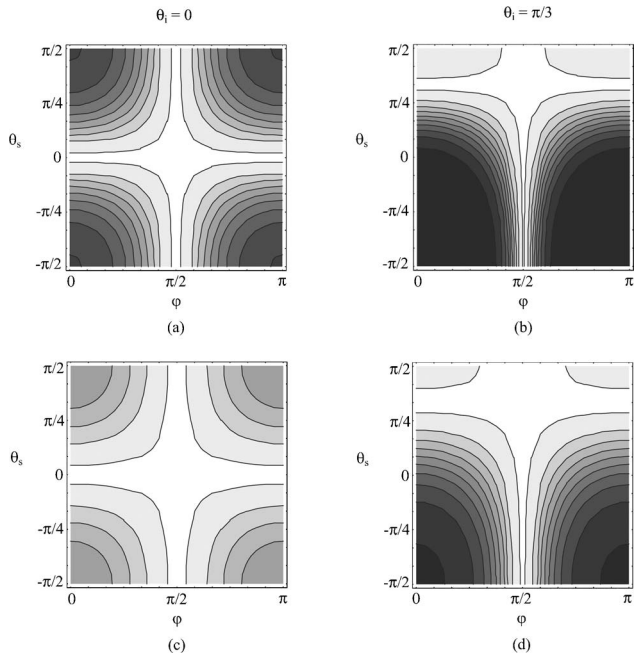

Fig. 3. Contour plots of the integrand of the coherent component of the general BRDF solution, which is proportional to the imaginary part of the plasma dispersion function, for two surfaces, for scattering in the specular plane at two incident angles, as functions of the scattering angle θ_s and the azimuthal correlation variable φ. The coherent component of the BRDF at θ_s is proportional to the integral over the corresponding horizontal line. Fixed parameters for these plots are $\bar{\lambda}=1\ \mu$m, $\rho_1=-0.005\ \mu\text{m}^{-1}$, $\rho_2=-0.005\ \mu\text{m}^{-2}$, and $\sigma=2$ [(a), (b)] or $\sigma=3$ [(c), (d)]. White represents 0, and dark shades represent negative values in gray-scale coding.

grand values across all of the plots. At a particular scattering angle θ_s the coherent component of the BRDF solution is proportional to the integral over the corresponding horizontal line. Note that $\xi L(\Gamma)(\cos\varphi)/\sqrt{\beta}\leq 0$ for Γ in the upper half of the complex plane.[44,70]

The characteristics of the general BRDF solution of relation (29) are illustrated in Section 3 through plots relevant to several applications of the forward and inverse scattering problems. Applications to the inverse problem are representative of the derived solution and do not utilize a search/optimization algorithm. The general solution is examined with variations of incident angle, surface roughness, illumination wavelength, and autocorrelation coefficients in the specular-plane bistatic and monostatic geometries, and over the full scattered hemisphere. Plots relevant to the forward problem are, where possible, compared qualitatively with published data due to surfaces with similar statistics.

3. RESULTS

The general BRDF solution given by relation (29) is dependent on eight parameters: the source (θ_i, ϕ_i, and $\bar{\lambda}$), the surface (σ_h, ρ_1, and ρ_2), and the observation parameters (θ_s and ϕ_s). Practical considerations and the mathematical assumptions of the model place restrictions on the surface parameters as follows: Referring to Eq. (9), without introducing higher derivatives of the surface autocorrelation, the assumption of large effective roughness can be approximately imposed as $\sigma_h \gg \bar{\lambda}/4\pi \cong 0.08\bar{\lambda}$. For the following (other than Figs. 7 and 10) the wavelength is fixed at $\bar{\lambda}=1\ \mu$m. The second derivative of the surface autocorrelation is fixed at $\rho_2=-0.005\ \mu\text{m}^{-2}$, and the first derivative is limited to the range $-0.05\ \mu\text{m}^{-1}\leq\rho_1\leq 0$, which places a conservative lower bound on the autocorrelation width of $a\gtrsim 25\ \mu$m. Multiple scattering, for which the model does not account, has been shown through the appearance of coherent backscattering to occur on surfaces for which the ratio $\sigma_h/a\gtrsim 0.2$.[79] Imposing the upper bound $\sigma_h<5\ \mu$m should therefore avoid surfaces with significant multiple scattering. The surface corresponding to the plots in Figs. 7 and 10 below is specified in the literature and has a larger autocorrelation width and larger roughness for which the assumptions of the model still hold. Computations of the two-dimensional plots of specular-plane bistatic scattering with $\pi/100$ resolution take approximately 30 s in Mathematica 5 un-

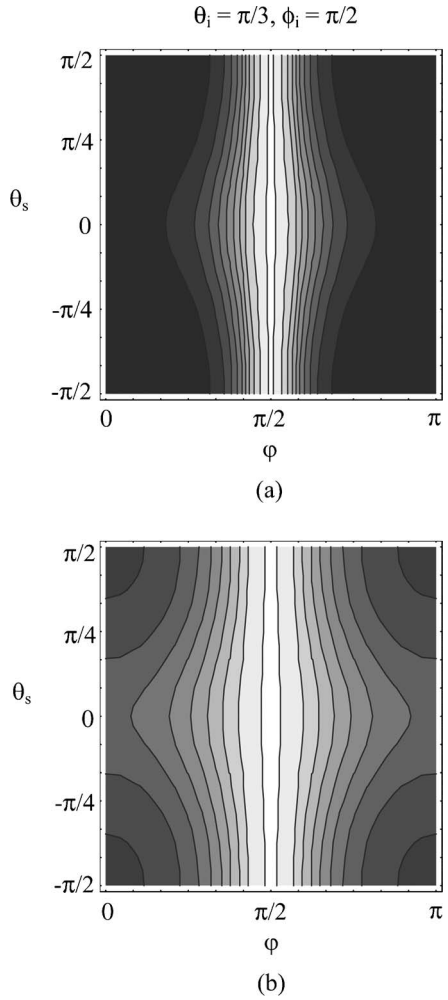

Fig. 4. Contour plots of the integrand of the coherent component of the general BRDF solution, which is proportional to the imaginary part of the plasma dispersion function, for the two surfaces specified in Fig. 3, for scattering normal to the specular plane, as functions of the scattering angle θ_s and the azimuthal correlation variable φ. Fixed parameters for these plots are (a) $\bar{\lambda}=1\ \mu$m, $\rho_1=-0.005\ \mu\text{m}^{-1}$, $\rho_2=-0.005\ \mu\text{m}^{-2}$, and $\sigma=2$ or (b) $\sigma=3$.

der the Microsoft Windows XP operating system on a 1.6 -GHz Intel Pentium 4 Mobile CPU with 512 Mbyte RAM.

The relatively little published data due to surfaces with wavelength-scale statistics against which the results of the model can be compared are summarized as follows, with the illumination wavelength and reported surface parameters given in the format $(\bar{\lambda}, \sigma_h, a)$ μm. The much-cited paper of O'Donnell and Méndez provides plots of the radiant intensity measured in the specular plane due to illumination at several angles θ_i of a gold surface with the well-defined statistics (0.6328, 2.3, 21) (Ref. 79); the autocorrelation of this surface is, however, almost exactly Gaussian, which relegates comparisons with the results of the current model to the pure Gaussian BRDF solution of relation (21). Several authors have reported measured backscattered or monostatic BRDFs due to surfaces with statistics in the range of interest, specifically Renau *et al.* for two aluminum surfaces characterized by (0.6328, 7, 50) and (0.6328, 1, 10) (Ref. 80) and Cheo and Renau for the former surface at the illumination wavelengths 0.6328, 3.39, and 10.6 μm.[81] Other data due to surfaces with wavelength-scale statistics are marginally relevant because the surfaces are either one-dimensionally rough[82] or nonconducting.[19] Considerably more data due to surfaces in this range are clearly needed.

A. Variation with Incident Angle

1. Specular-Plane Bistatic

The specular-plane variation with the incident angle θ_i of the general BRDF solution is illustrated in Fig. 5 for three surfaces. For the effective roughness $\sigma=0.75$ fixed in Fig. 5, the radiant intensity due to the Gaussian-like surface of Fig. 5(a) maintains a nearly Gaussian form symmetric about the specular direction for small θ_i, which is consistent with the data reported by O'Donnell and Méndez.[79] The maximum intensity scattered by the surfaces considered in Fig. 5 decreases with θ_i, although the opposite behavior, maximum scattered intensity increasing with θ_i, is predicted by the model (but not shown) for surfaces with the fixed parameters of Fig. 5 and larger $|\rho_1|$. A familiar feature of the scattered intensity of sufficiently rough surfaces is the so-called off-specular peak, which is a shift of the mode or the angle of maximum intensity away from the specular direction toward the surface normal. In the coherence interpretation of the BRDF the off-specular peak occurs naturally as the coherent component decreases. Figure 5 suggests that the shift of the mode is dependent on the functional form of the surface autocorrelation. For instance, at $\theta_i=30°$ the mode due to the Gaussian-like surface of Fig. 5(a) is in the specular direction, while the mode due to the Cauchy-like surface of Fig. 5(c) is shifted by more than 5°.

Significant features of the general BRDF solution evident in Fig. 5 are the lobes or wings that persist far from the specular direction in scattering by the intermediate to Cauchy-like surfaces. This feature, which is most relevant at low relative intensities far from the specular direction, is commonly observed in measurements, for instance in the (*s*-polarized) specular-plane intensity, plotted logarithmically in Fig. 6, due to a milled, black-anodized aluminum plate illuminated with $\bar{\lambda}=1.06$ μm (*s*-polarized) at $\theta_i=30°$.[83] In Fig. 6 the squares represent the measured data points, which are fitted without optimization by the derived BRDF solution for the intermediate surface given by the solid curve. Some popular models[1,2,30] account for the wings observed in many BRDF measurements by adding to the Gaussian BRDF a so-called diffuse or Lamber-

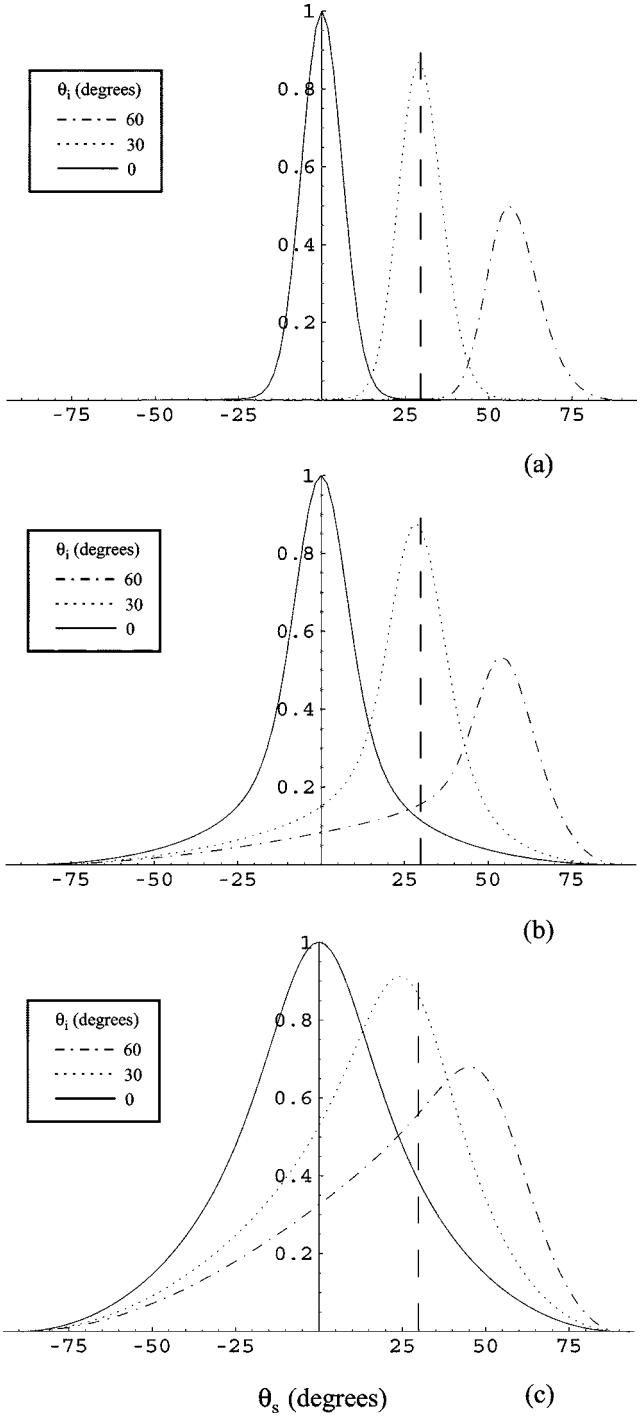

Fig. 5. Variation with incident angle θ_i of the general solution for the radiant intensity in the specular plane due to (a) a Gaussian-like ($\rho_1=-0.0001$ μm^{-1}), (b) an intermediate ($\rho_1=-0.005$ μm^{-1}), and (c) a Cauchy-like ($\rho_1=-0.02$ μm^{-1}) surface. The units on the vertical axes are normalized across the plots, and $\rho_2=-0.005$ μm^{-2}, $\sigma_h=0.75$ μm, and $\bar{\lambda}=1$ μm are fixed. The vertical dashed lines mark the specular direction for $\theta_i=30°$.

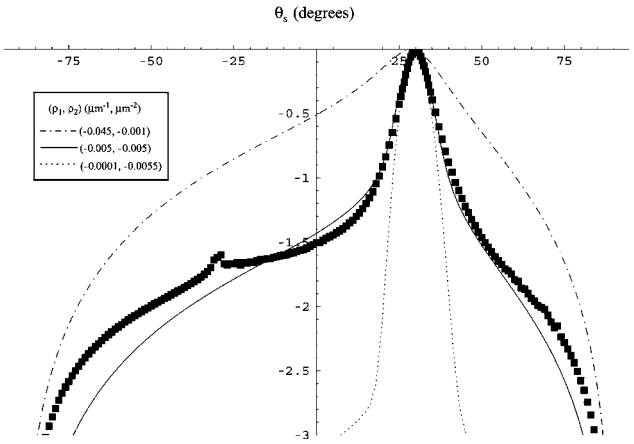

Fig. 6. Derived solution for the radiant intensity (solid curve) fit to data (squares) due to a milled, black-anodized aluminum surface with the illumination at $\theta_i = 30°$ and the detection both in the *s*-polarization component. The dotted and dotted–dashed curves represent the derived radiant intensities due to Gaussian-like and Cauchy-like surfaces, respectively, with the same autocorrelation lower bound as that for the surface corresponding to the solid curve. Logarithms of the measured and derived radiant intensities are plotted following independent normalizations, and $\sigma_h = 0.35$ μm and $\bar{\lambda} = 1$ μm are fixed. The results imply that the surface autocorrelation function is non-Gaussian.

tian term, which is commonly ascribed to multiple scattering. Our results suggest that the wings observed in many BRDF measurements are due not necessarily to multiple scattering but rather to non-Gaussian surface autocorrelation functions with nonvanishing gradients near the origin.

A significant feature of the general BRDF solution illustrated by Fig. 6 is the considerable variation in the angular energy distribution among surfaces with similar statistics σ and a but different autocorrelation coefficients. Specifically, the three model curves in Fig. 6 have the same effective roughness $\sigma = 0.35$ and the same autocorrelation lower bound $a \gtrsim 19$ μm, yet the corresponding BRDFs differ by up to 3 orders of magnitude. This behavior of the general solution may explain the large discrepancies in the predictions of earlier models applied to the inverse problem of topographical mapping from BRDF data. The fits of models based on the linear autocorrelation approximation to lunar radar returns radically overestimate the size of lunar surface features.[51] The solution of the current model that most closely resembles the solutions of earlier models based on the linear autocorrelation approximation is that due to the Cauchy-like surface [see relation (22)]. With reference to Fig. 6, the solution due to the Cauchy-like surface with the correct statistics is in poor agreement with the data. If the current model were restricted to only Cauchy-like surfaces, as are models based on the linear autocorrelation approximation, then agreement with the data in Fig. 6 could be achieved only by assuming a much smaller coefficient $|\rho_1|$ (with $\rho_2 = 0$), which implies a surface autocorrelation much larger than 19 μm, i.e., the fit of the solution due to the Cauchy-like surface overestimates the size of the surface features. The addition of a possibly small Gaussian component, made possible by the general quadratic autocorrelation expansion, may therefore provide significant improvements over previous results in topographical mapping of such surfaces.

2. Monostatic

The backscattered or monostatic BRDF is most relevant in laser-radar applications, where the source and detector are usually collocated on the same platform. The monostatic BRDF gives the backscattered cross section as a function of the orientation of the target planar reflector.[1,2] The monostatic geometry is specified notationally as $\bar{\mathbf{k}}_s = -\bar{\mathbf{k}}_i$, or $\theta_s = \theta_i$ and $\phi_s = \phi_i = 0$. Figure 7 illustrates the monostatic radiant intensities due to three surfaces according to the general solution of relation (29) with fixed illumination and surface parameters corresponding to those reported by Renau *et al.*[80] As in Fig. 6, logarithmic plots reveal dramatic differences among the BRDFs due to surfaces with similar statistics ($\sigma = 7$ μm and $a \gtrsim 58$ μm) but different autocorrelation coefficients, particularly in the backscattered intensities far from the specular direction. The monostatic BRDF due to the surface corresponding to the solid curve in Fig. 7 is in qualitative agreement with the previously published data[80] for incident angles up to around 40°, beyond which the derived solution for this surface underestimates the backscattered intensity. All of the surfaces corresponding to the plots in Fig. 7 are Gaussian-like ($|\rho_2| > |\rho_1|$); however, the monostatic BRDF due to the purely Gaussian surface ($\rho_1 = 0$) compares very poorly with the published data. The previously published data against which the model curves are compared in Fig. 7 have been previously fitted to about the same level of accuracy by a model based on parabolic perturbation of a set of Gaussian-distributed microfacets using an apparently large, albeit undisclosed, number of arbitrary coefficients.[84]

The results of Fig. 7 demonstrate the extremely sensitive dependence of the monostatic BRDFs due to surfaces with large effective roughness on the surface autocorrelation coefficients and emphasize the need to allow for even minuscule deviations from the Gaussian autocorrelation in the development of credible scattering models. It is also worth noting that the general monostatic BRDF solutions

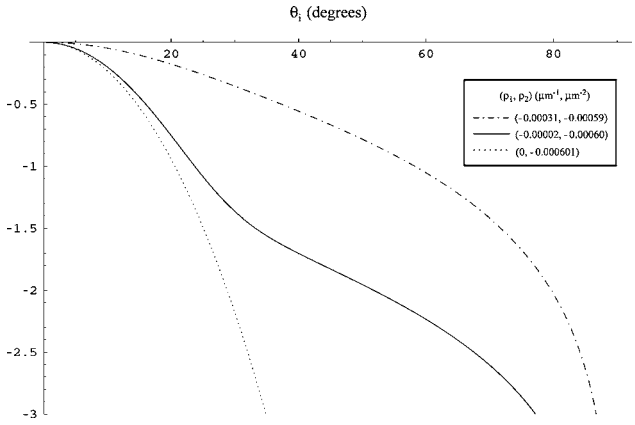

Fig. 7. Derived monostatic radiant intensities due to three surfaces with the same autocorrelation lower bound and $\sigma_h = 7$ μm illuminated with $\bar{\lambda} = 0.6328$ μm. The logarithms of the derived radiant intensities are plotted following independent normalizations.

due to Cauchy-like surfaces with large autocorrelation widths (not shown) agree qualitatively with previously published radar data due to planetary surfaces.[48–50]

B. Variation with Surface Roughness

1. Specular-Plane Bistatic

Figure 5 indicates the dependence of the mode angle of the general BRDF solution on the surface autocorrelation coefficients at fixed surface roughness. The mode shift is expected to increase as the coherent component of the BRDF solution decreases due to increasing roughness. Figure 8 illustrates this effect as well as the dramatic dependence of the mode shift on the autocorrelation coefficients. For $\sigma=2$ the radiant intensity due to the Cauchy-like surface in Fig. 8(c) is centered near the surface normal, resembling the incoherent solution, while the intensity due to the Gaussian-like surface in Fig. 8(a) is centered less than 10° from the specular direction $\theta_s=45°$. We emphasize that the phenomenon of the off-specular peak is not necessarily reliant on shadowing, as has been claimed based on microfacet analyses,[35] but is rather the result of coherence loss in the ensemble-average scattered surface field. As discussed in Subsection 2.B, coherence loss is accompanied by an increasing evanescent component that removes energy from the BRDF, an effect also evident in Fig. 8.

2. Full Hemisphere

Figure 9 illustrates the logarithmic variation over the full scattered hemisphere of the model radiant intensities due to intermediate surfaces at two roughness values. The surface corresponding to Fig. 9(a) is the same as that which generates the BRDF solution fit to the specular-plane data due to the aluminum surface in Fig. 6. The longitudinal lines in the plots of Fig. 9 correspond to the azimuth ϕ_s in 10° increments, the latitudinal lines correspond to the elevation θ_s in 0.9° increments, and the incident direction ($\theta_i=30°$) is indicated by the vertical arrows. The ripple at $\theta_s\approx 20°$ in the backscattered radiant intensity due to the smoother surface [Fig. 9(a)] is likely a numerical artifact.

C. Spectral Variation

Wavelength scaling of the BRDF is important for many applications. For instance, for HEL applications the BRDF is usually measured in a laboratory at wavelengths different from those used in the field, in which case the accuracy of radiometric simulations and analyses are squarely dependent on an understanding of the spectral variations of the BRDF. For broadband applications such as passive photometry, illumination design, and computer graphics and vision, wavelength-scaling algorithms preclude time-consuming tabulations of the BRDF over the source spectrum.

Certain of our results provide insights into the diffractive spectral variation of the BRDF. In particular, with reference to Eqs. (1) and (5) and relation (21), the pure Gaussian BRDF solution is found to be diffractively achromatic or independent of wavelength except for the reflected emittance $\bar{M}_r$, which is a result that has been noted before.[32] By contrast, the Cauchy solution of relation (22) is highly dispersive and nonmonotonic, with wavelength dependence proportional to $\bar{\lambda}^2/[1+(c\xi\bar{\lambda})^2]^{3/2}$ with $c=1/8\pi\sigma_h^2|\rho_1|$ and a maximum intensity at the wavelength $\bar{\lambda}_{\max}(\xi)=\sqrt{2}/c\xi$. These results suggest that the diffractive spectral variation of the BRDF is strongly dependent on the surface autocorrelation coefficients. Figure 10 depicts the diffractive spectral variation of the BRDF so-

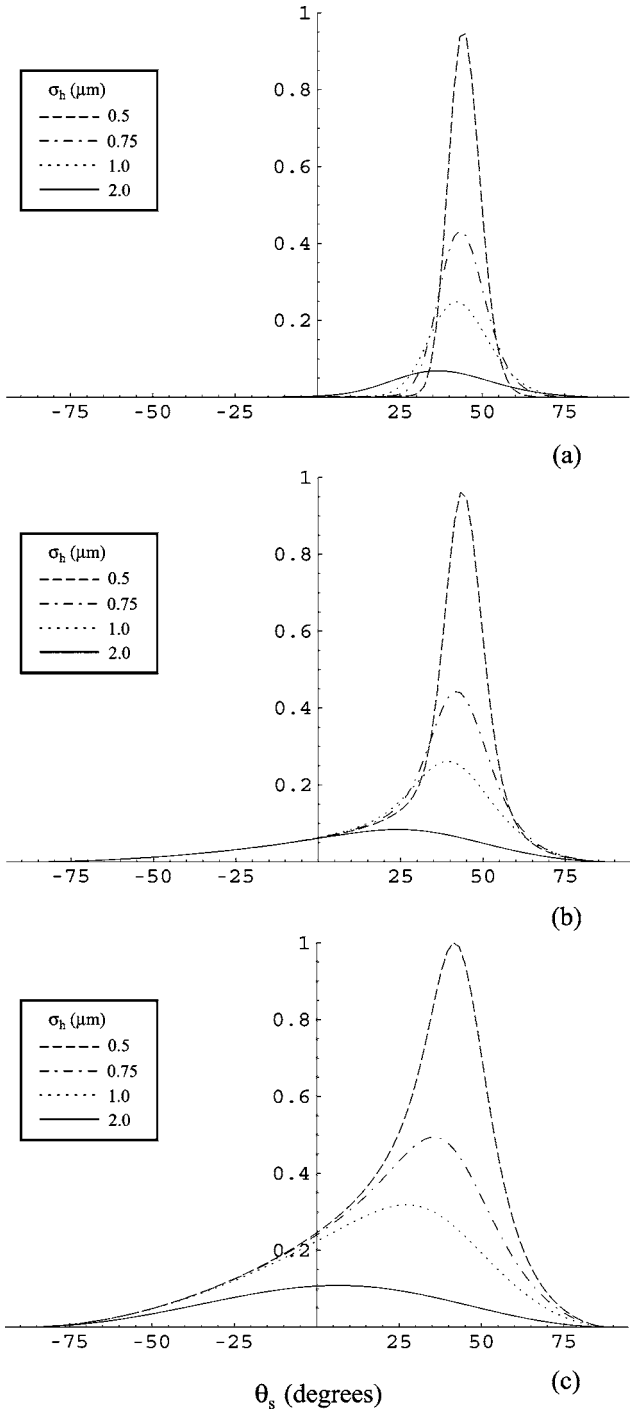

Fig. 8. Variation with roughness σ_h of the general solution for the radiant intensity in the specular plane ($\theta_i=45°$) due to (a) a Gaussian-like ($\rho_1=-0.0001\ \mu\text{m}^{-1}$), (b) an intermediate ($\rho_1=-0.005\ \mu\text{m}^{-1}$), and (c) a Cauchy-like ($\rho_1=-0.02\ \mu\text{m}^{-1}$) surface. The units on the vertical axes are normalized across the plots, and $\rho_2=-0.005\ \mu\text{m}^{-2}$ and $\bar{\lambda}=1\ \mu\text{m}$ are fixed.

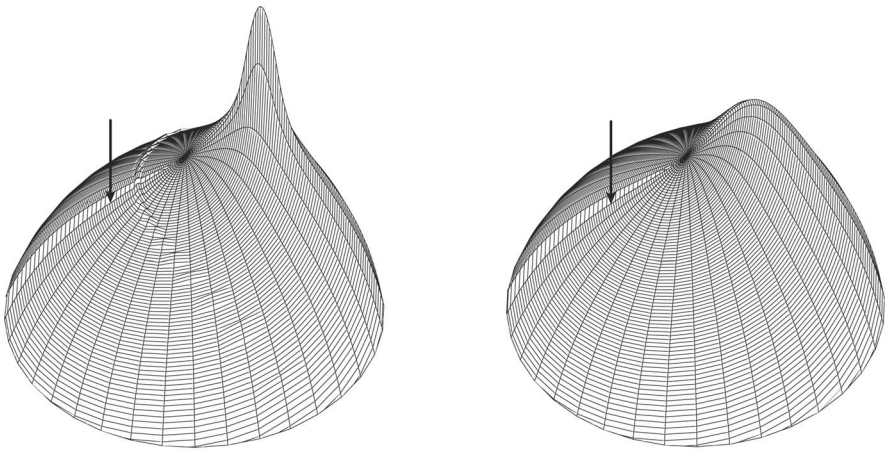

Fig. 9. Full-hemisphere plots of the derived general solution for the radiant intensity due to two surfaces. The longitudinal lines correspond to scattered azimuth angle ϕ_s, the latitudinal lines correspond to scattered elevation angle θ_s, and the incident direction ($\theta_i = 30°$) is indicated by the vertical arrows. Fixed parameters are $\bar{\lambda} = 1\ \mu$m, $\rho_1 = -0.005\ \mu\text{m}^{-1}$, $\rho_2 = -0.005\ \mu\text{m}^{-2}$, and $\sigma_h = 0.35\ \mu$m (a) or $\sigma_h = 1\ \mu$m (b). The logarithms of the radiant intensities are plotted over the range $[-3, 0]$ following coupled normalization.

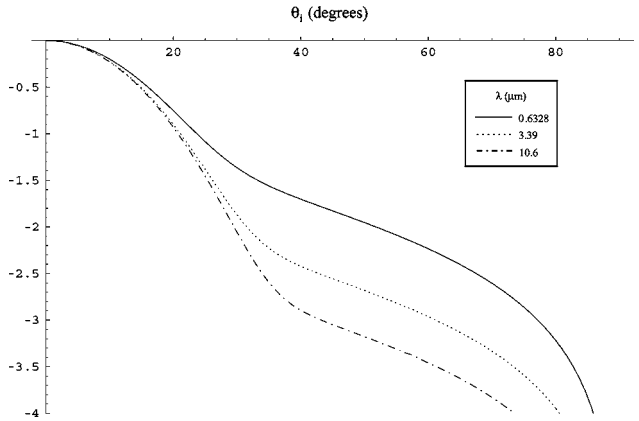

Fig. 10. Derived monostatic radiant intensities due to a surface illuminated at three wavelengths. Fixed surface parameters are $\sigma_h = 7\ \mu$m, $\rho_1 = -0.00002\ \mu\text{m}^{-1}$, and $\rho_2 = -0.0006\ \mu\text{m}^{-2}$. The logarithms of the derived radiant intensities are plotted following coupled normalizations.

lution in monostatic plots at three wavelengths, motivated by previously published data due to an aluminum surface.[81] The autocorrelation coefficients used to generate the model curves in Fig. 10 are those determined in Fig. 7, although as in Fig. 7 the fits are representative without use of an optimization routine. The spectral trend of the solution agrees with that of the data, although as in Fig. 7 the solution somewhat underestimates the data. Cheo and Renau noted that the measured monostatic BRDF at normal incidence is independent of wavelength provided that $\sigma_h/\lambda \gtrsim 0.25$. The general BRDF solution is consistent with this observation, as evidenced by the normalization of all of the curves in Fig. 10 by the solution at normal incidence for $\bar{\lambda} = 0.6328\ \mu$m. In fact, relation (29) reveals that the diffractive portion of the general BRDF solution is achromatic in the specular direction irrespective of the illumination and surface parameters. We should, however, emphasize that the general solution and the plots in Fig. 10 do not include spectral variation of the reflected emittance $\bar{M}_r$ that occurs due to surfaces of nonperfect conductors.

4. CONCLUSIONS

In this paper some established concepts from the theories of scattering and coherence are utilized to develop a model for the description of scattering from perfectly conducting surfaces with wavelength-scale statistics. The model holds in principle for surfaces with any value of large effective roughness provided that shadowing and multiple scattering are negligible. Previously published models and measurements of surface scattering have concentrated primarily on either very smooth surfaces, for which theory is well developed and verified,[85] or rougher surfaces that exhibit multiple-scattering effects such as coherent backscattering.[79,86–88] Despite the ubiquity of surfaces with statistics on the scale of the wavelength in many of the applications noted earlier, progress in the description of scattering from such surfaces has been limited. Perhaps as a consequence, relatively few measurements of scattering from such surfaces have been reported.

While the ultimate value of coherence theory in scattering analysis is perhaps yet to be determined, several formalisms and interpretations introduced in this paper appear to extend the understanding of surface scattering. The BRDF solution is derived as the sum of an incoherent and a coherent component, the latter of which is proportional to an integral of the plasma dispersion function. Such a decomposition allows for the interpretation of scattering phenomena such as nonspecular maxima and energy conservation in the context of coherence theory, where analogous phenomena of primary radiation sources have been thoroughly investigated. The solution also suggests an analogy between surface scattering and wave propagation in plasmas that may prove useful. It is noted that the standard tangent-plane approximation for the scattered field is incompatible with the coherence approach, and the alternative phase-screen approximation

allows for the consideration of surfaces with large and/or discontinuous slopes. The general BRDF solution interpolates between the well-known Gaussian and Cauchy solutions, behavior previously derived apparently only on the assumption of fractal surfaces.[89]

Several effects that the current model does not describe should motivate future investigations. Preliminary comparisons with data suggest that shadowing may be relevant at large incident angles. It may be possible to incorporate shadowing and other effects into the model through specification of the amplitude moment in Eq. (7), effectively extending the phase screen to an amplitude–phase screen. Efforts are under way to extend the model to the description of anisotropic roughness and electromagnetic (vector)-wave scattering through application of recent developments in electromagnetic coherence theory.[41] Throughout the development of this paper the reflected emittance $\bar{M}_r$ has remained a free parameter, although it obviously depends on the wavelength and the optical constants of the surface material. It may be possible to determine $\bar{M}_r$ by using the results of the current model with global constraints such as Helmholtz reciprocity.[90] Such an approach would effectively determine the reflected emittance from surface correlations, in contrast to conventional attempts to determine emittance from surface slopes, which typically rely on the dubious application of the Fresnel formulas to reflection from tangent planes.

APPENDIX A

This appendix demonstrates the derivation of Eq. (3), the generalized Van Cittert–Zernike (VCZ) theorem in the form applicable to BRDF model development. We begin with the expression for the scalar optical field u at a point P inside a volume bounded by a known surface S, which is given by the Rayleigh–Sommerfeld (R-S) diffraction formula as[28,73]

$$u(P) = \frac{j}{\lambda}\int\int_S u\frac{\exp(jkr)}{r}(\hat{\mathbf{n}}\cdot\hat{\mathbf{r}})\mathrm{d}S, \tag{A1}$$

where $r\hat{\mathbf{r}}$ is the vector from the surface to the point P and $\hat{\mathbf{n}}$ is the surface normal. The R-S diffraction formula allows derivation of the propagation law for the mutual intensity, which for a common class of coherence states is known as the generalized VCZ theorem. Goodman provides a thorough reference on the VCZ theorem.[61]

In temporally stationary, narrowband light, i.e., $\Delta\nu \ll \bar{\nu}$, if the time delay τ is much less than the coherence time τ_c, the coherence function $\Gamma(\mathbf{x}_1,\mathbf{x}_2,\tau)\equiv\langle u(\mathbf{x}_1,t)u^*(\mathbf{x}_2,t-\tau)\rangle$ takes the form

$$\Gamma(\mathbf{x}_1,\mathbf{x}_2,\tau)\cong\Gamma(\mathbf{x}_1,\mathbf{x}_2,0)\exp(-2\pi j\bar{\nu}\tau) = J(\mathbf{x}_1,\mathbf{x}_2)\times\exp(-2\pi j\bar{\nu}\tau), \tag{A2}$$

where J is known as the mutual intensity and describes only the effects of spatial coherence. In regions where relation (A2) is satisfied, the light is said to be *quasi-monochromatic* with the center frequency $\bar{\nu}$.[91] Using the R-S formula of Eq. (A1), we express the propagation of the mutual intensity from a planar surface S to the pair of points (P_1,P_2) as

$$J(P_1,P_2)\equiv\langle u(P_1)u^*(P_2)\rangle = \frac{1}{\bar{\lambda}^2}\int\int_S\int\int_S\langle u(\mathbf{x}_1)u^*(\mathbf{x}_2)\rangle\frac{\exp[j\bar{k}(r_1-r_2)]}{r_1r_2}\times(\hat{\mathbf{n}}_1\cdot\hat{\mathbf{r}}_1)(\hat{\mathbf{n}}_2\cdot\hat{\mathbf{r}}_2)\mathrm{d}\mathbf{x}_1\mathrm{d}\mathbf{x}_2, \tag{A3}$$

with $\mathbf{x}\equiv x\hat{\mathbf{x}}+y\hat{\mathbf{y}}$ as the two-dimensional vector over the planar surface S. Equation (A3) is reiterated as Goodman's Eq. 5.4-8.[61]

Several simplifications of Eq. (A3) occur in the context of BRDF theory. First, only the propagated intensity is of interest, and therefore $P_1=P_2=P$. The scattering surface is assumed to be globally planar, and the surface S is taken as a phantom planar surface just above the actual surface, which implies that $\hat{\mathbf{n}}_1=\hat{\mathbf{n}}_2=\hat{\mathbf{z}}$. Also, the point P is in the Fraunhofer, or far, zone of the illuminated portion of the surface S, which leads to the usual Fraunhofer approximations. Specifically, with reference to Fig. 1, $\hat{\mathbf{n}}_1\cdot\hat{\mathbf{r}}_1=\hat{\mathbf{n}}_2\cdot\hat{\mathbf{r}}_2=\cos\theta$, $1/r_1r_2=1/Z^2$ in amplitude, and $r=Z-\hat{\mathbf{s}}\cdot\mathbf{x}$ in phase, where $\hat{\mathbf{s}}$ is the direction of the scattered wave vector $\mathbf{k}_s$. With these simplifications the average *irradiance* at the point P is derived from Eq. (A3) as

$$\langle I(P)\rangle\equiv J(P,P)\cong\frac{\cos^2\theta}{(Z\bar{\lambda})^2}\int\int_S\int\int_S J(\mathbf{x}_1,\mathbf{x}_2)\times\exp[j\bar{k}\hat{\mathbf{s}}\cdot(\mathbf{x}_2-\mathbf{x}_1)]\mathrm{d}\mathbf{x}_1\mathrm{d}\mathbf{x}_2. \tag{A4}$$

$\langle I(P)\rangle$ is the power per unit area on a small detector centered in the direction $\hat{\mathbf{s}}$ at the distance Z from the surface. It is convenient to eliminate Z by defining the *radiant intensity* $\langle I(\bar{\mathbf{k}}_s)\rangle\equiv Z^2\langle I(P)\rangle$, which is the power per steradian along $\hat{\mathbf{s}}$. In the context of BRDF theory $\langle\cdot\rangle$ in Eqs. (A3) and (A4) represents an average over both time and an independent, identically distributed (IID) ensemble of surfaces or media.

Fields scattered by rough surfaces typically satisfy two assumptions regarding the mutual intensity $J(\mathbf{x}_1,\mathbf{x}_2)$ on the surface. It is first assumed that the normalized mutual intensity function γ on the surface depends only on coordinate differences, that is,

$$\gamma(\Delta\mathbf{x}) = \frac{J(\mathbf{x}_1,\mathbf{x}_2)}{\sqrt{I(\mathbf{x}_1)I(\mathbf{x}_2)}}, \tag{A5}$$

which will be satisfied if the surface heights are described by a stationary random process.[92] The conventions $\mathbf{x}_2=\mathbf{x}_1-\Delta\mathbf{x}$ and $\Delta\mathbf{x}\cdot\hat{\mathbf{x}}\geq 0$ are adopted for mutual intensities that satisfy Eq. (A5), which characterize sources known as statistically homogeneous or shift invariant. The second assumption is that the ensemble-average reflected irradiance varies negligibly over the coherence area of the scattered surface field, in which case

$$J(\mathbf{x}_1,\mathbf{x}_2)\cong I(\bar{\mathbf{x}})\gamma(\Delta\mathbf{x}), \tag{A6}$$

where $\bar{\mathbf{x}}$ is the average vector between $\mathbf{x}_1$ and $\mathbf{x}_2$. A field that satisfies relation (A6) is known as a *quasi-homogeneous* field. In the context of BRDF theory the quasi-homogeneous condition will be satisfied under flood

illumination of a surface with spatially uniform roughness on a scale greater than the illumination wavelength, i.e., for $\sigma \gtrsim 1$. Surfaces with specular reflection components, for which $\sigma \ll 1$, do not satisfy the quasi-homogeneous condition. Inserting the mutual intensity under the quasi-homogeneous condition into Eq. (A4) and changing to sum and difference surface variables produces

$$\langle I(\bar{\mathbf{k}}_s)\rangle \cong \frac{\cos^2\theta}{\bar{\lambda}^2}\int\int_S I(\bar{\mathbf{x}})\mathrm{d}\bar{\mathbf{x}}\int\int_S \gamma(\Delta\mathbf{x})\exp(-j\bar{\mathbf{k}}_s\cdot\Delta\mathbf{x})\mathrm{d}\Delta\mathbf{x}$$

$$= \frac{\mathcal{A}\bar{I}_r\cos^2\theta}{\bar{\lambda}^2}\int\int_S \gamma(\Delta\mathbf{x})\exp(-j\bar{\mathbf{k}}_s\cdot\Delta\mathbf{x})\mathrm{d}\Delta\mathbf{x}, \qquad \text{(A7)}$$

where $\bar{I}_r$ is the average reflected irradiance over the illuminated area $\mathcal{A}$. Equation (A7), which is identical to Eq. (3), is the generalized VCZ theorem as applicable to BRDF model development. The reflected irradiance is distinguished from the irradiance on the detector by introducing the average *emittance* of the surface reflection as $\bar{M}_r \equiv \bar{I}_r$. In this context the emittance is averaged over time, medium, and area.

ACKNOWLEDGMENTS

The authors thank Laura Ulibarri and Mike Wilkes at AFRL/DES, Lewis DeSandre at AFRL/DET, Emil Wolf at the University of Rochester, Oscar Bruno at Caltech, David Reicher at S-Systems Corporation, and David Wellems at Applied Technology Associates for technical discussions, and Joseph Costantino at AFRL/MLBT for providing original data. This research was supported by the U.S. Air Force Research Laboratory under contract FA9451-04-C-0353.

B. G. Hoover's e-mail address is hoover@advanced-optical.com.

REFERENCES AND NOTES

1. O. Steinvall, "Effects of target shape and reflection on laser radar cross sections," Appl. Opt. **39**, 4381–4391 (2000).
2. O. Steinvall and T. Carlsson, "Three-dimensional laser radar modelling," in*Laser Radar Technology and Applications VI*, G. W. Kamerman, ed., Proc. SPIE **4377**, 23–24 (2001).
3. A. I. Carswell, "Advances in laser ranging," in *Laser Radar Technology for Remote Sensing*, C. Werner, ed., Proc. SPIE **5240**, 1–9 (2004).
4. W. C. Snyder and Z. Wan, "BRDF models to predict spectral reflectance and emissivity in the thermal infrared," IEEE Trans. Geosci. Remote Sens. **36**, 214–225 (1998).
5. M. Kaasalainen, K. Muinonen, and T. Laakso, "Shapes and scattering properties of large irregular bodies from photometric data," Opt. Express **8**, 296–301 (2001).
6. S. Kaasalainen, J. Piironen, M. Kaasalainen, A. W. Harris, K. Muinonen, and A. Cellino, "Asteroid photometric and polarimetric phase curves: empirical interpretation," Icarus **161**, 34–46 (2003).
7. D. Fontani, F. Francini, G. Longobardi, and P. Sansoni, "Optical control of surface finish," Opt. Lasers Eng. **32**, 459–472 (2000).
8. P. A. Smith, D. A. van Veldhuizen, and K. S. Keppler, "Modeling and simulation tools for high-energy laser safety applications," in *Enabling Technology for Simulation Science V*, A. F. Sisti and D. A. Trevisani, eds., Proc. SPIE **4367**, 478–485 (2001).
9. S. H. C. P. McCall, "The importance of scatter in stray light analysis," Opt. Photonics News **12**(11), 40–47 (2001).
10. F. Drago and K. Myszkowski, "Validation proposal for global illumination and rendering techniques," Comput. Graphics **25**, 511–518 (2001).
11. M. S. Gilmore, R. Castaño, T. Mann, R. C. Anderson, E. D. Mjolsness, R. Manduchi, and R. S. Saunders, "Strategies for autonomous rovers at Mars," J. Geophys. Res. **105**, 29223–29237 (2000).
12. O. G. Cula and K. J. Dana, "3D texture recognition using bidirectional feature histograms," Int. J. Comput. Vis. **59**, 33–60 (2004).
13. T. Weyrich, H. Pfister, and M. Gross, "Rendering deformable surface reflectance fields," IEEE Trans. Vis. Comput. Graph. **11**, 48–58 (2005).
14. J. Dorsey and P. Hanrahan, "Digital materials and virtual weathering," Sci. Am. **282**(2), 64–71 (2000).
15. F. Bernardini, I. M. Martin, and H. Rushmeier, "High-quality texture reconstruction from multiple scans," IEEE Trans. Vis. Comput. Graph. **7**, 318–332 (2001).
16. C. Rocchini, P. Cignoni, C. Montani, and R. Scopigno, "Acquiring, stitching, and blending diffuse appearance attributes on 3D models," Visual Comput. **18**, 186–204 (2002).
17. J. Meseth, G. Müller, and R. Klein, "Reflectance field based real-time, high-quality rendering of bidirectional texture functions," Comput. Graphics **28**, 105–112 (2004).
18. A. Ishimaru and J. S. Chen, "Scattering from very rough metallic and dielectric surfaces: a theory based on the modified Kirchhoff approximation," Waves Random Media **1**, 25–34 (1991).
19. G. Macelloni, G. Nesti, P. Pampaloni, S. Sigismondi, D. Tarchi, and S. Lolli, "Experimental validation of surface scattering and emission models," IEEE Trans. Geosci. Remote Sens. **38**, 459–469 (2000).
20. O. P. Bruno, A. Sei, and M. Caponi, "High-order high-frequency solutions of rough surface scattering problems," Radio Sci. **37**, 10.1029/2000 RS002551 (2002).
21. M. Saillard and A. Sentenac, "Rigorous solutions for electromagnetic scattering from rough surfaces," Waves Random Media **11**, R103–R137 (2001).
22. T. M. Elfouhaily and C.-A. Guérin, "A critical survey of approximate scattering wave theories from random rough surfaces," Waves Random Media **14**, R1–R40 (2004).
23. S. O. Rice, "Reflection of electromagnetic waves from slightly rough surfaces," Commun. Pure Appl. Math. **4**, 351–378 (1951).
24. J. Stover, *Optical Scattering: Measurement and Analysis* (McGraw-Hill, 1990).
25. J. A. Ogilvy, *Theory of Wave Scattering from Random Rough Surfaces* (Hilger/IOP, 1991).
26. G. S. Agarwal, "Scattering from rough surfaces," Opt. Commun. **14**, 161–166 (1975).
27. J. A. Sánchez-Gil and M. Nieto-Vesperinas, "Light scattering from random rough dielectric surfaces," J. Opt. Soc. Am. A **8**, 1270–1286 (1991).
28. P. Beckmann and A. Spizzichino, *The Scattering of Electromagnetic Waves from Rough Surfaces* (Pergamon, 1963).
29. E. R. Méndez, E. E. Garcia-Guerrero, H. M. Escamilla, A. A. Maradudin, T. A. Leskova, and A. V. Shchegrov, "Photofabrication of random achromatic optical diffusers for uniform illumination," Appl. Opt. **40**, 1098–1108 (2001).
30. X. D. He, K. E. Torrance, F. X. Sillion, and D. P. Greenberg, "A comprehensive physical model for light reflection," Comput. Graph. **25**, 175–186 (1991).
31. S. Silver, "Scattering and diffraction," in *Microwave Antenna Theory and Design*, S. Silver, ed. (McGraw-Hill, 1949), Chap. 5.
32. J. C. Leader, "Bidirectional scattering of electromagnetic waves from rough surfaces," J. Appl. Phys. **42**, 4808–4816 (1971).
33. J. C. Leader, "Analysis and prediction of laser scattering

from rough-surface materials," J. Opt. Soc. Am. **69**, 610–628 (1979).
34. R. D. Kodis, "A note on the theory of scattering from an irregular surface," IEEE Trans. Antennas Propag. **AP-14**, 77–82 (1966).
35. K. E. Torrance and E. M. Sparrow, "Theory for off-specular reflection from roughened surfaces," J. Opt. Soc. Am. **57**, 1105–1114 (1967).
36. D. E. Barrick, "Rough surface scattering based on the specular point theory," IEEE Trans. Antennas Propag. **AP-16**, 449–454 (1968).
37. M. Ashikhmin, S. Premože, and P. Shirley, "A microfacet-based BRDF generator," in *Proceedings of ACM SIGGRAPH 2000* (www.siggraph.org), pp. 65–74.
38. K. Ivanova, M. A. Michalev, and O. I. Yordanov, "Numerical study of scattering by rough surfaces with intermediate and large scale roughness," Radio Sci. **26**, 505–510 (1991).
39. F. Gori, "Matrix treatment for partially polarized, partially coherent beams," Opt. Lett. **23**, 241–243 (1998).
40. E. Wolf, "Unified theory of coherence and polarization of random electromagnetic beams," Phys. Lett. A **312**, 263–267 (2003).
41. O. Korotkova, B. G. Hoover, V. L. Gamiz, and E. Wolf, "Coherence and polarization properties of far-fields generated by quasi-homogeneous electromagnetic sources," J. Opt. Soc. Am. A **22**, 2547–2556 (2005).
42. W. Gautschi, "Error function and Fresnel integrals," in *Handbook of Mathematical Functions*, 9th ed., M. Abramowitz and I. A. Stegun, eds. (Dover, 1972), Chap. 7.
43. W. J. Thompson, "Numerous neat algorithms for the Voight profile function," Comput. Phys. **7**, 627–631 (1993).
44. R. J. Wells, "Rapid approximation to the Voight/Faddeeva function and its derivatives," J. Quant. Spectrosc. Radiat. Transf. **62**, 29–48 (1999).
45. D. L. Jordan, G. D. Lewis, and E. Jakeman, "Emission polarization of roughened glass and aluminum surfaces," Appl. Opt. **35**, 3583–3590 (1996).
46. A. K. Fung, "Theory of radar scatter from rough surfaces, bistatic and monostatic, with application to lunar radar return," J. Geophys. Res. **69**, 1063–1073 (1964).
47. P. Beckmann, "Scattering by composite rough surfaces," Proc. IEEE **53**, 1012–1015 (1965).
48. A. K. Fung and R. K. Moore, "Effects of structure size on moon and earth radar returns at various angles," J. Geophys. Res. **69**, 1075–1081 (1964).
49. W. K. Klemperer, "Angular scattering law for the moon at 6-meter wavelength," J. Geophys. Res. **70**, 3798–3800 (1965).
50. J. V. Evans, "Radar studies of planetary surfaces," Annu. Rev. Astron. Astrophys. **7**, 201–248 (1969).
51. D. E. Barrick, "Unacceptable height correlation coefficients and the quasi-specular component in rough surface scattering," Radio Sci.**5**, 647–654 (1970).
52. K. E. Warnick and D. V. Arnold, "Generalization of the geometrical-optics scattering limit for a rough conducting surface," J. Opt. Soc. Am. A **15**, 2355–2361 (1998).
53. J. W. Goodman, "Statistical properties of laser speckle patterns," in *Laser Speckle and Related Phenomena*, 2nd enlarged ed., J. C. Dainty, ed. (Springer-Verlag, 1984), Chap. 2.
54. A review of the radiometric units and notation used in this paper is provided in E. L. Dereniak and D. G. Crowe, *Optical Radiation Detectors* (Wiley, 1984).
55. A. Walther, "Radiometry and coherence," J. Opt. Soc. Am. **58**, 1256–1259 (1968).
56. E. Wolf and W. H. Carter, "Angular distribution of radiant intensity from sources of different degrees of spatial coherence," Opt. Commun. **13**, 205–209 (1975).
57. L. Mandel and E. Wolf, *Optical Coherence and Quantum Optics* (Cambridge U. Press, 1995), Chap. 5.7.
58. J. C. Leader, "Similarities and distinctions between coherence theory relations and laser scattering phenomena," Opt. Eng. (Bellingham) **19**, 593–601 (1980).
59. D. D. Duncan, D. V. Hahn, and M. E. Thomas, "Physics-based polarimetric BRDF models," in *Optical Diagnostic Methods for Inorganic Materials III*, L. M. Hanssen, ed., Proc. SPIE **5192**, 129–140 (2003).
60. B. G. Hoover and V. L. Gamiz, "Diffractive bidirectional reflectance distributions of surfaces with large effective roughness in one dimension," in *Laser Radar Techniques for Atmospheric Sensing*, U. N. Singh, ed., Proc. SPIE **5575**, 137–142 (2004).
61. J. W. Goodman, *Statistical Optics* (Wiley, 1985), Chap. 5.
62. $\mathbf{x}$ and $\Delta\mathbf{x}$ represent two-dimensional vectors in the plane of the average surface, i.e., $\mathbf{x}=x\hat{\mathbf{x}}+y\hat{\mathbf{y}}$.
63. T. Karabacak, Y. Zhao, M. Stowe, B. Quayle, G.-C. Wang, and T.-M. Lu, "Large-angle in-plane light scattering from rough surfaces," Appl. Opt. **39**, 4658–4668 (2000).
64. See Ref. 51 and references therein.
65. G. A. Korn and T. M. Korn, *Mathematical Handbook for Scientists and Engineers* (McGraw-Hill, 1961), Chap. 5.
66. J. D. Jackson, *Classical Electrodynamics*, 2nd ed. (Wiley, 1975), Chap. 9.
67. J. D. Gaskill, *Linear Systems, Fourier Transforms, and Optics* (Wiley, 1978), Chap. 9.
68. I. S. Gradshteyn and I. M. Ryzhik, *Table of Integrals, Series and Products*, corrected and enlarged ed. (Academic, 1980), 6.631(4).
69. I. S. Gradshteyn and I. M. Ryzhik, *Table of Integrals, Series and Products*, corrected and enlarged ed. (Academic, 1980), 6.623(2).
70. B. D. Fried and S. D. Conte, *The Plasma Dispersion Function: The Hilbert Transform of the Gaussian* (Academic, 1961). Note that the function defined in this reference has its real and imaginary parts switched relative to the plasma dispersion function defined in Refs. 42–44 and 71.
71. V. N. Faddeeva and N. M. Terent'ev, *Tables of Values of the Function* $w(z)=e^{-z^2}(1+2i/\sqrt{\pi}\int_0^z e^{t^2}dt)$ *for Complex Argument*, V. A. Fok ed., translated by D. G. Fry (Pergamon, 1961).
72. V. Bagini, F. Frezza, M. Santarsiero, G. Schettini, and G. Schirripa-Spagnolo, "Generalized Bessel–Gauss beams," J. Mod. Opt. **43**, 1155–1166 (1996).
73. J. W. Goodman, *Introduction to Fourier Optics*, 2nd ed. (McGraw-Hill, 1996), Chap. 2.
74. W. H. Carter and E. Wolf, "Coherence properties of Lambertian and non-Lambertian sources," J. Opt. Soc. Am. **65**, 1067–1071 (1975).
75. H. P. Baltes, B. Steinle, and G. Antes, "Spectral coherence and the radiant intensity from statistically homogeneous and isotropic planar sources," Opt. Commun. **18**, 242–246 (1976).
76. The meanings of the terms "high frequency" and "low frequency" in coherence theory are unfortunately essentially opposite their meanings in scattering theory. Use of these terms in this context is therefore avoided.
77. Derivatives of the δ function are considered in T. B. A. Senior and J. L. Volakis, *Approximate Boundary Conditions in Electromagnetics* (IEEE Press, 1995).
78. E. W. Weisstein, "Erf," from *MathWorld–A Wolfram Web Resource*, http://mathworld.wolfram.com/Erf.html.
79. K. A. O'Donnell and E. R. Méndez, "Experimental study of scattering from characterized random surfaces," J. Opt. Soc. Am. A **4**, 1194–1205 (1987).
80. J. Renau, P. K. Cheo, and H. G. Cooper, "Depolarization of linearly polarized EM waves backscattered from rough metals and inhomogeneous dielectrics," J. Opt. Soc. Am. **57**, 459–466 (1967).
81. P. K. Cheo and J. Renau, "Wavelength dependence of total and depolarized backscattered laser light from rough metallic surfaces," J. Opt. Soc. Am. **59**, 821–826 (1969).
82. E. Marx and T. V. Vorburger, "Direct and inverse problems for light scattered by rough surfaces," Appl. Opt. **29**, 3613–3626 (1990).
83. L. Brainard, W. Lynn, D. Ramer, and W. Shemano, "Optical measurements facility," Air Force Research Laboratory, Materials & Manufacturing Directorate, Rep. AFRL-ML-WP-TR-1999-4142 (1999).
84. C. C. Sung and W. D. Eberhardt, "Explanation of the

experimental results of light backscattered from a very rough surface," J. Opt. Soc. Am. **68**, 323–328 (1978).
85. A review of theory and measurements in the small-roughness regime is provided in J. M. Elson and J. M. Bennett, "Vector scattering theory," Opt. Eng. (Bellingham) **18**, 116–124 (1979).
86. A. J. Sant, J. C. Dainty, and M.-J. Kim, "Comparison of surface scattering between identical, randomly rough metal and dielectric diffusers," Opt. Lett. **14**, 1183–1185 (1989).
87. M.-J. Kim, J. C. Dainty, A. T. Friberg, and A. J. Sant, "Experimental study of enhanced backscattering from one- and two-dimensional random rough surfaces," J. Opt. Soc. Am. A **7**, 569–577 (1990).
88. N. C. Bruce and J. C. Dainty, "Multiple scattering from rough dielectric and metal surfaces using the Kirchhoff approximation," J. Mod. Opt. **38**, 1471–1481 (1991).
89. M. K. Shepard and B. A. Campbell, "Radar scattering from a self-affine fractal surface: near-nadir regime," Icarus **141**, 156–171 (1999).
90. W. C. Snyder, "Reciprocity of the bidirectional reflectance distribution function (BRDF) in measurements and models of structured surfaces," IEEE Trans. Geosci. Remote Sens. **36**, 685–691 (1998).
91. It is possible to dispense with the quasi-monochromatic conditions by using the cross-spectral density $W(\mathbf{x}_1, \mathbf{x}_2, \nu) = \int \Gamma(\mathbf{x}_1, \mathbf{x}_2, \tau) \exp(2\pi j \nu \tau) \mathrm{d}\tau$ rather than the coherence function, thus proceeding in the space–frequency rather than the space–time domain. Under the quasi-monochromatic conditions these two approaches are essentially equivalent.
92. Some authors use the symbol μ to represent the normalized mutual intensity function.[61] We reserve μ for the analogous correlation function in the space–frequency domain.[57]